ELSEVIER

Ceramics International 26 (2000) 721–725

CERAMICS INTERNATIONAL

Anomalous cyclic fatigue-crack propagation behavior of small cracks in monolithic, grain-bridging ceramics

C.J. Gilbert [a], Y.S. Han [b], D.K. Kim [b], R.O. Ritchie [a,*]

[a] *Materials Sciences Division, Lawrence Berkeley National Laboratory, and Department of Materials Science and Mineral Engineering, University of California, Berkeley, CA 94720, USA*

[b] *Department of Material Science and Engineering, Korea Advanced Institute of Science and Technology, Yusong-Gu, Taejon 305-701, South Korea*

Received 29 July 1999; received in revised form 7 September 1999; accepted 17 November 1999

Abstract

Cyclic fatigue properties of two monolithic, high-toughness SiC ceramics were examined, with emphasis placed on differences between long- (> 3 mm) and small-crack (< 250 μm) behavior. Studies were performed on two microstructures in which sintering additives were systematically varied. Small cracks were initiated with Vickers indents placed on the tensile surfaces of beams, and crack extension was monitored optically under an applied cyclic load. For small cracks, high growth rates which exhibited a negative dependence on the far-field driving force were observed. Such behavior was rationalized both in terms of indent-induced residual stresses and the relative size of cracks compared to bridging zone lengths.

Keywords: C. Fatigue; C. Fracture; C. Mechanical properties; D. SiC

1. Introduction

Over the past decade, considerable research effort has focused on improving the toughness of monolithic ceramics [1]. A particularly successful strategy involves the promotion of highly elongated, heterogeneous microstructures (often referred to as in situ toughening). Silicon nitride is the earliest example of this approach [2], and more recent work on silicon carbide [3–5] has demonstrated its broad applicability. As cracks propagate through such microstructures, provided that fracture is intergranular, the elastic and frictional tractions generated from the contact of opposing crack faces (generally termed "grain bridging") act to reduce the driving force in the immediate vicinity of the crack tip. As one might expect, the degree of shielding is enhanced in larger, more elongated microstructures. Indeed, long-crack fracture toughnesses approaching 10 MPa$\sqrt{m}$ have been achieved in optimally designed Si_3N_4 and SiC [2,5].

An important limitation associated with grain bridging involves the length scales over which it operates. In order for a saturated bridging zone to develop, the peak (or long-crack) fracture toughness is not reached until cracks are substantially larger than microstructural dimensions. This scaling effect gives rise to the ubiquitous "resistance-curve" always associated with tough ceramics [1]. Because the saturation distance (or bridging zone length) is typically on the order of ~1 mm, long-crack toughnesses do not apply to microstructurally small cracks. Cracks in this size domain are known to dictate important mechanical properties such as strength, wear, and machinability, and in most structural components the initial flaw distribution is indeed physically small. Moreover, cyclic-fatigue crack growth rates measured using long-crack specimens may overestimate resistance to subcritical crack propagation. Recent work has demonstrated that microstructurally small cracks propagate at substantially higher growth rates than long cracks at equivalent driving forces under both quasi-static and cyclic loading conditions in a number of monolithic ceramics and their composites [6–9].

Therefore, the primary objective of the present study is to quantify cyclic fatigue-crack growth rates of small cracks in several high-toughness SiC microstructures. Particular emphasis is placed on the differences between long-crack (through-thickness cracks with initial lengths > 3 mm) and small-crack (indent-initiated surface cracks with initial lengths < 200 μm) growth rates.

* Corresponding author. Tel.: +1-510-642-0417; fax: +1-510-486-4995.

E-mail address: roritchie@lbl.gov (R.O. Ritchie).

0272-8842/00/$ - see front matter
PII: S0272-8842(00)00010-9

Results are rationalized in terms of the relative size of cracks compared to both bridging-zone lengths and the extent of indent-induced residual stress fields.

2. Experimental procedures

2.1. Materials

Studies were performed on two high-toughness silicon carbide microstructures. The first, termed ABC-SiC [5,10], was processed by hot pressing submicron β-SiC powder, mixed with 3 wt% Al, 0.6 wt% B, and 4 wt% Apiezon wax (converted to ~2 wt% C upon pyrolysis), at 1900°C for 1 h at 50 MPa under flowing argon [5]. The resulting microstructure (Fig. 1a) consisted of an interlocking network of elongated and plate-like primarily α-phase (4H polytype) grains, typically 5.5 ± 2.4 μm long by 0.7 ± 0.2 μm wide surrounded by a ~1 nm thick amorphous Al-containing grain-boundary phase. Details of the microstructure and properties are reported elsewhere [5,10]. ABC-SiC has an ambient-temperature strength (four-point bend) of 650 ± 40 MPa and a fracture toughness, K_c, of ~9.1 MPa$\sqrt{m}$, the latter resulting from extensive crack bridging by the plate-like grains. Such bridging gives rise to a resistance curve (*R*-curve), which increases to a long-crack fracture toughness of ~9.1 MPa$\sqrt{m}$ after ~600 μm of stable crack extension [10].

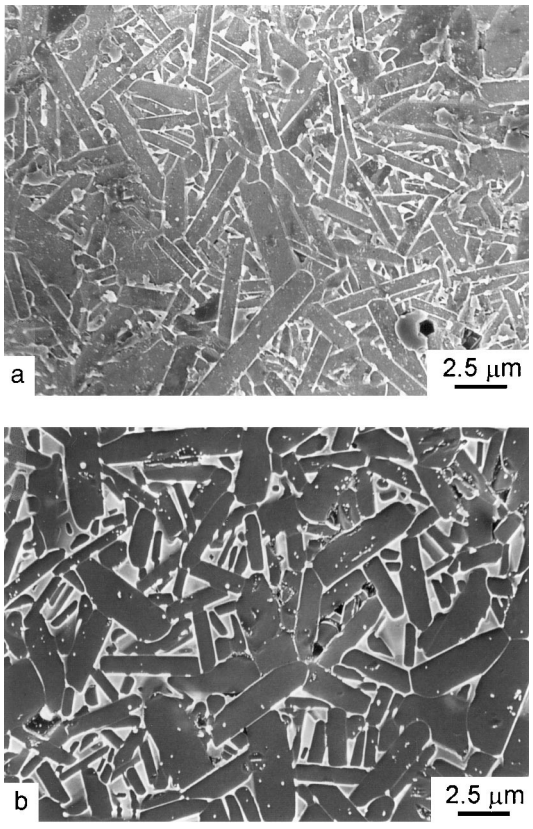

Fig. 1. Scanning electron micrographs of the microstructures of (a) ABC-SiC and (b) 6A4Y-SiC. Surfaces were plasma etched prior to observation.

The second silicon carbide was processed by mixing β-SiC powder with 6 wt% Al_2O_3 and 4 wt% Y_2O_3 and hot-pressing at 1950°C for 0.5 h under 25 MPa pressure and flowing argon. Fully dense billets were subsequently annealed at 1950°C for 3 h to promote the formation of elongated grains. The resulting microstructure (Fig. 1b), termed 6A4Y-SiC, also consisted of high aspect-ratio grains ~5 μm long and ~1 μm wide surrounded by substantial amounts of amorphous grain-boundary phase. 6A4Y-SiC has a long-crack fracture toughness of ~6.2 MPa$\sqrt{m}$, achieved after ~250 μm of stable crack extension. This again results from a primarily intergranular fracture path which gives rise to significant crack bridging by the elongated microstructure.

2.2. Long-crack measurements

Long-crack cyclic fatigue-crack growth properties were determined in a controlled room-air environment (22°C, 45% relative humidity) on disc-shaped compact-tension DC(T) specimens (thickness, B~3 mm and width, W~15 mm) machined from as-sintered billets. Specimens were cycled under stress intensity (K) control, with a test frequency of 25 Hz (sinusoidal waveform) at a constant load ratio (ratio of minimum to maximum load) of $R = 0.1$, using computer-controlled, servo-hydraulic mechanical testing machines, in general accordance with ASTM standard E647. To obtain a wide spectrum of growth rates, samples were first cycled with a decreasing stress-intensity range, ΔK, (at a normalized K-gradient of 0.09 mm^{-1}) until measured growth rates were less than 10^{-10} m/cycle; the value of the stress-intensity range at this point was used to operationally define the fatigue threshold stress intensity, $K_{max,TH}$, below which long cracks are essentially dormant. After threshold determination, specimens were cycled under increasing ΔK conditions with the same K-gradient in order to determine growth rates up to ~10^{-7} m/cycle. Prior to data collection, samples were fatigue pre-cracked for several millimeters beyond the as-machined notch. Thereafter, crack lengths were monitored using unloading elastic-compliance measurements with a 350 Ω strain gauge attached to the back-face of the specimen; crack lengths were also checked periodically using a traveling microscope. Data are presented in terms of the growth rate per cycle, da/dN, as a function of the maximum stress intensity of the loading cycle, K_{max}, the latter being computed using standard linear-elastic handbook solutions.

2.3. Small-crack measurements

Small-crack cyclic fatigue-crack growth rates were determined by monitoring indent-initiated surface

cracks on the tensile surface of bend beams (nominal cross sections of ~3×3 mm, and lengths ranging from ~30 to 50 mm). Prior to testing, the tensile surface of each beam was polished to a ~1 μm diamond finish, and the edges were beveled. A series of Vickers indents were placed along the axis of each beam (on the tensile surface) at a fixed indent load, P. The indent load was sustained for ~10 s, and center-to-center separations of at least 2 mm were maintained in order to avoid interaction between indents. Indentation loads were varied from 49 to 90 N, giving initial surface crack lengths, $2a$, of ~175 to 250 μm. The multiple indents on a given specimen (typically three to four) allowed for the initiation of multiple small cracks, each experiencing a different applied bending moment. More data could therefore be collected per specimen. Indented specimens were cycled in bending in a controlled room-air environment (22°C, 45% relative humidity), with a sinusoidal loading frequency of 25 Hz and load ratio, $R=0.1$. Each specimen was cycled until failure or crack arrest.

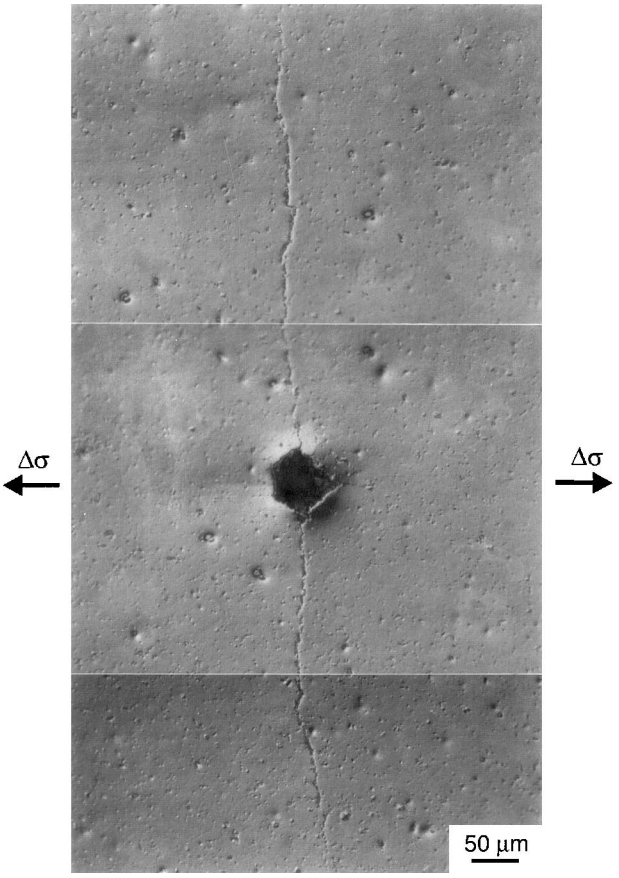

Fig. 2. An optical micrograph (with Nomarski filter) of a replicated indent in ABC-SiC after exposure to ~2.1×10^4 fatigue cycles ($P=70$ N, $\sigma_{max}=340$ MPa). Note the extensive crack growth normal to the applied cyclic stress.

Fatigue tests were periodically interrupted to examine each indent for crack growth. Tests were always interrupted after the first cycle and subsequently every 10^2–10^4 cycles until failure. Changes in crack length could be quantified to within ~5 μm. Following final fracture, the crack depth-to-half-surface-length ratios, c/a, were determined by examining fracture surfaces in the scanning electron microscope (typically c/a ~0.65, where c is the crack depth).

The stress intensity factor due to bending was computed at the surface of the specimen using linear-elastic solutions for three-dimensional surface cracks given elsewhere [11]. Crack growth rates at each indent were calculated from plots of the surface crack length, $2a$, versus the number of fatigue cycles, N; measured cyclic fatigue-crack growth rates, da/dN, ranged from 10^{-5} to 10^{-12} m/cycle. The data are presented in terms of the maximum stress intensity of the loading cycle, K_{max}, with $c/a=0.65$.

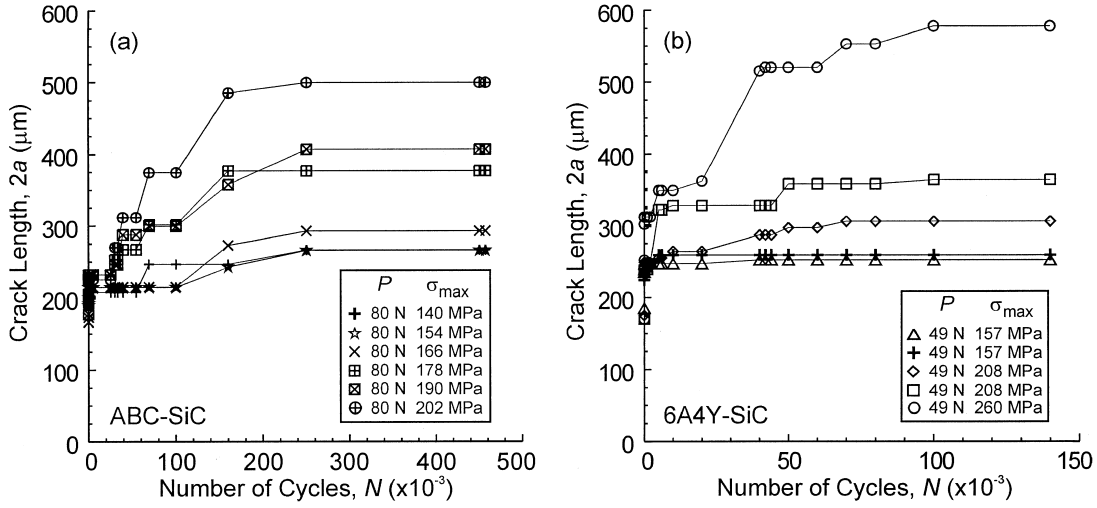

Fig. 3. Surface crack length, $2a$, is plotted in terms of loading cycles, N, for (a) ABC-SiC and (b) 6A4Y-SiC. For the sake of clarity, not all ABC-SiC data are shown.

To account for the effect of the indent-induced residual stress field, the local contribution, K_{rd}, to the total applied stress intensity was computed from $K_{rd} = \chi P a^{-3/2}$, where χ is a factor which depends on indent geometry, as well as on elastic and plastic properties of the material [12]; a typical value of $\chi \sim 0.084$ is used here [13]. The total stress intensity in fatigue at the maximum point in the loading cycle, K_{tot}, is therefore given by the superposition, $K_{tot} = K_{max} + K_{rd}$. Note that while K_{max} increases with increasing crack length (at a fixed bending stress), K_{rd} decreases. For small crack sizes where the indent-induced residual stress field dominates, the total driving force, K_{tot}, initially decreases with increasing crack length. As the crack grows away from the indent, however, the applied bending field dominates and K_{tot} begins to increase with crack length [12].

3. Results and discussion

For indent-initiated surface cracks in both the ABC-SiC and 6A4Y-SiC, substantial stable crack growth was observed at far-field driving forces well below the long-crack thresholds. An example is shown in Fig. 2 (ABC-SiC) for an indent-crack exposed to $\sim 2.1 \times 10^4$ fatigue cycles ($R = 0.1$, 25 Hz) at a constant maximum applied bending stress, σ_{max}, of 340 MPa ($P = 70$ N). Crack growth initiated at a far-field applied driving force of $K_{max} \sim 4.3$ MPa$\sqrt{m}$ compared to the long-crack threshold, $K_{max,TH} \sim 7.1$ MPa$\sqrt{m}$ [10]. (Notice that crack extension occurred only in a direction normal to the applied bending stress).

Crack length, $2a$, is plotted as a function of cycles, N, for a number of these indent-initiated surface cracks in

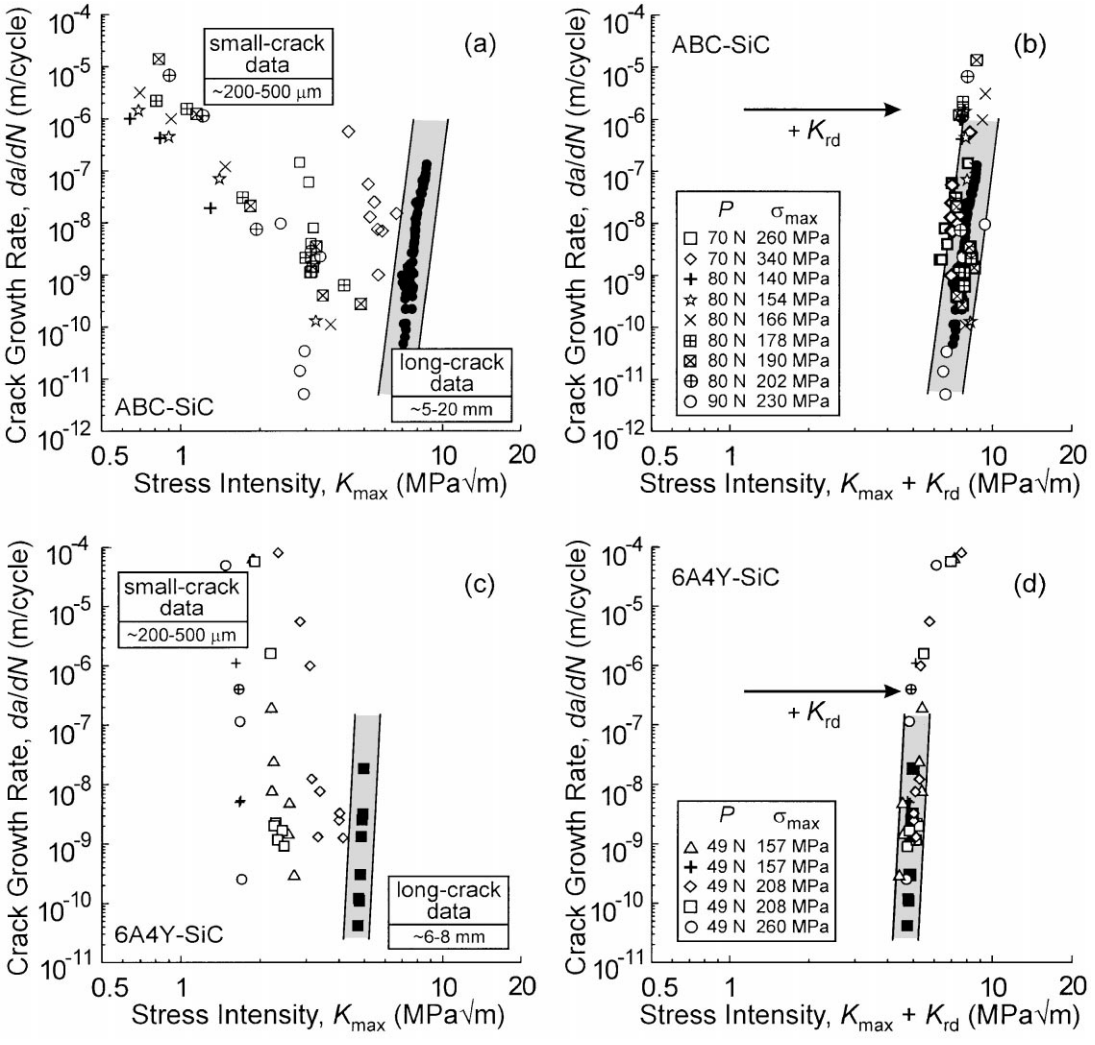

Fig. 4. Cyclic fatigue-crack growth rates, da/dN, are plotted for both long cracks (shaded regions) and small cracks (open symbols) in (a), (b) for the ABC-SiC and in (c), (d) for the 6A4Y-SiC. In (a), (c) data are plotted as function of the maximum applied stress intensity, K_{max}, and in (b), (d) as function of the total driving force, $K_{max} + K_{rd}$.

both the ABC-SiC (Fig. 3a) and the 6A4Y-SiC (Fig. 3b) over a wide range of indent loads and bending stresses. Several points should be noted here. First, despite the constant far-field applied stress condition (tabulated for each indent in Fig. 3), crack-growth rates tended to decrease with increasing crack length. This was due to the dominance of the local residual stress field, K_{rd}, which decreases with increasing crack size. Second, as one would expect, flaws subjected to higher applied bending stresses (at a fixed indent load) generally grew at higher growth rates. Third, significant fluctuations in growth rates were observed as the cracks propagated. This large degree of scatter is expected for small cracks as crack growth is markedly affected by local microstructural inhomogeneities of dimensions comparable with crack sizes.

The data in Fig. 3 were subsequently used to determine crack-growth rates as a function of the maximum applied driving force, K_{max}, for both the ABC-SiC (Fig. 4a) and the 6A4Y-SiC (Fig. 4c). Included in these plots are the long-crack data measured using through-thickness cracks in DC(T) specimens (filled symbols in the shaded regions). In every case, small cracks exhibited higher crack-growth rates than long cracks when plotted in terms of the far-field applied driving force, K_{max}; indeed, crack extension was detected well below the long-crack thresholds in every case. Moreover, unlike the long-crack growth rates, the small-crack data exhibited a negative dependence on the far-field driving force, and the data displayed no unique dependence on K_{max}. Rather, growth rates were also sensitive to the maximum applied stress, σ_{max}.

After accounting for the indent-induced residual stress field, however, the small-crack data nearly collapsed onto the long-crack data for both the ABC-SiC (Fig. 4b) and the 6A4Y-SiC (Fig. 4d). The success of this normalization suggests that in this case the indent-induced residual stresses are the primary source of the apparently anomalous behavior. These observations are consistent with those seen in an Al_2O_3/SiC_w composite [6], monolithic Al_2O_3 and Si_3N_4 [7,8], and transformation-toughened ceramics such as Ce-PSZ [9]. Had a lack of bridging indeed been a significant cause for the apparently anomalous small-crack behavior, small-crack growth rates would still exceed long-crack growth rates even after accounting for indent-induced residual stresses. This does not appear to be the case. Presumably these indent cracks are large enough relative to the bridging zone lengths to benefit from a substantial amount of bridging-induced crack-tip shielding.

4. Summary and conclusions

A comparison of crack propagation behavior of indent-initiated small cracks and through-thickness long cracks has been made in two high-toughness SiC microstructures. The measurements establish that flaws greater than ~200 μm in size behave like long through-thickness cracks. Indeed, after accounting for indent-induced residual stresses, their behavior matches the long-crack DC(T) data extremely well. We expect, however, that flaws at even smaller length scales (e.g. tens of microns) will exhibit anomalous behavior, and this is the subject of future studies.

Acknowledgements

Work on the Al, B, C-based SiC was supported by the Director, Office of Energy Research, Office of Basic Energy Sciences, Materials Sciences Division of the US Department of Energy under Contract No. DE-AC03-76SF00098. Additional support to facilitate collaboration between the Korean and U.S. groups on the Al_2O_3/Y_2O_3-based SiC was provided by the U.S. National Science Foundation through their Division of International Programs under Grant No. INT-9507653. Thanks are also due to Mr. Q. Tran for experimental assistance.

References

[1] A.G. Evans, J. Am. Ceram. Soc. 73 (1990) 187.
[2] C.W. Li, J. Yamanis, J. Am. Ceram. Soc. 75 (1992) 1777.
[3] S.K. Lee, C.H. Kim, J. Am. Ceram. Soc. 77 (1994) 1655.
[4] N.P. Padture, J. Am. Ceram. Soc. 77 (1994) 519.
[5] J.J. Cao, W.J. Moberlychan, L.C. De Jonghe, C.J. Gilbert, R.O. Ritchie, J. Am. Ceram. Soc. 79 (1996) 461.
[6] R.H. Dauskardt, M.R. James, J.R. Porter, R.O. Ritchie, J. Am. Ceram. Soc. 75 (1992) 759.
[7] A. Ueno, H. Kishimoto, S. Ookawara, T. Kondo, A. Yamamoto, J. Soc. Mat. Sci. Jpn 43 (1994) 183.
[8] T. Hoshide, T. Ohara, T. Yamada, Int. J. Fract 37 (1988) 47.
[9] D.C. Cardona, C.J. Beevers, Scripta Metall 23 (1989) 945.
[10] C.J. Gilbert, J.J. Cao, W.J. Moberly Chan, L.C. De Jonghe, R.O. Ritchie, Acta Mater. 44 (1996) 3199.
[11] I.S. Raju, S.N. Atluri, J.C. Newman Jr., Stress-intensity factors for small surface and corner cracks in plates, in: R. P. Wei, R. P. Gangloff (Eds.), Fracture Mechanics — Perspectives and Directions, ASTM STP 1020, American Society for Testing and Evaluation, Philadelphia, 1989.
[12] B.R. Lawn, Fracture of Brittle Solids, Cambridge University Press, New York, 1993.
[13] C.J. Gilbert, J.J. Cao, W.J. Moberly Chan, L.C. De Jonghe, R.O. Ritchie, Am. Ceram. Soc. 80 (1997) 2253.